CrossMark

ORIGINAL PAPER

Experimental study of the azimuthal performance of 3D acoustic transmitter stations

Xiao-Hua Che[1,2] · Wen-Xiao Qiao[1,2] · Xiao-Dong Ju[1,2] · Jun-Qiang Lu[1,2] ·
Jin-Ping Wu[1,2] · Ming Cai[1,2]

Abstract Better well logging techniques for geologic investigations are urgently needed to identify and evaluate complex reservoirs. We describe a new type of 3D transmitter station with corresponding circuits and bodies. They can be used in a promising new technique of acoustic reflection well logging, that features better azimuthal detection capabilities, as well as better investigation depth. The transmitter stations consist of three-level subarrays that can radiate acoustic energy in any required azimuth of 3D space by circularly exciting various combinations at different levels. We tested the 3D acoustic transmitter stations and obtained laboratory directivity measurements with the 3D acoustic transmitter stations for the first time. The results show that the 3-dB beam width in the horizontal plane ranges from 59° to 67° as a result of phase-delayed excitation. The main beam is steered in the vertical plane at a deflection angle that ranges from 0° to 16° when the delay time of the excitation pulse between each pair of adjacent arc arrays is gradually adjusted. The 3-dB beam width is equal to 11°, whereas the deflection angle in the vertical plane is equal to 14°. Each of the four third-level subarrays in the same circumferential direction display consistent horizontal and vertical directivities, thus satisfying the requirements of azimuthal acoustic reflection logging.

✉ Xiao-Hua Che
  aclab@cup.edu.cn

1   State Key Laboratory of Petroleum Resources and
    Prospecting, China University of Petroleum, Beijing 102249,
    China

2   Key Laboratory of Earth Prospecting and Information
    Technology, China University of Petroleum, Beijing 102249,
    China

Edited by Jie Hao

1 Introduction

In conventional monopole acoustic well logging, symmetrical acoustic sources facilitate shallow investigations, but they fail to detect fractures and small-scale geologic structures near boreholes, and they cannot evaluate the azimuthal properties of the formations around the boreholes (Haldorsen et al. 2006a). The acoustic waves reflected by the near-borehole interfaces with non-continuous acoustic impedance are obtained through acoustic reflection logging (Hornby 1989; Ellis et al. 1996; Esmersoy et al. 1997, 1998; Chang et al. 1998; Yamamoto et al. 1998; 1999). Migration imaging techniques that are similar to those used in seismic exploration are then employed to visualize small-scale geologic structures from a few meters to dozens of meters away from boreholes (Yamamoto et al. 2000; Tang 2004; Pistre et al. 2005; Li et al. 2008; Chai et al. 2009; Tang et al. 2007). Acoustic reflection logging generally facilitates more in-depth investigation than conventional acoustic logging, and it also yields images with higher resolution than those obtained through seismic exploration. Thus, this method is promising for future complex reservoir exploration.

The Borehole Acoustic Reflection Survey developed by Schlumberger employs monopole acoustic sources that radiate acoustic energy evenly in the circumferential direction. Monopole sources with single receivers cannot detect reflector azimuths, which is why Schlumberger used multi-receivers for their survey (Yamamoto et al. 2000; Al Rougha et al. 2005; Maia et al. 2006; Haldorsen et al. 2006b, 2010; Jervis et al. 2012). The acoustic reflection

well logging tool (Zhao et al. 2004; Chai et al. 2009) developed by Bohai Drilling of the Dagang Oilfield Well Logging Branch employs a linear phased-array transmitter that is also a symmetrical acoustic source. This tool can identify high-angle fractures within 10 m of the well; however, reflector azimuth information cannot be extracted because of the axial symmetry of radiated acoustic fields.

In dipole remote acoustic reflection imaging, dipole acoustic sources are used to image small-scale, near-borehole geologic structures (Tang 2004; Patterson et al. 2008; Tang et al. 2007; Tang and Patterson 2009; Tang and Wei 2012a, b; Wei et al. 2013). Although low-frequency dipole acoustic sources provide for more thorough radial investigations, the directivities of the sources and the receivers limit the azimuthal resolution with 180° azimuthal ambiguity. Furthermore, the logging results are related to the positions of the logging tool in boreholes, and the sampling time is long.

Therefore, well logging tools with azimuthal resolution and remote-detecting functions are urgently required to invert the detailed formation information that is essential to geologic evaluations, reservoir characterizations, and oil-in-place assessments. To eliminate the azimuth ambiguity of single-well imaging, Zhang and Hu proposed a technique based on the pressure and displacement component, and they validated it by simulated examples (Zhang and Hu; 2014), whereas Gong et al. proposed a method using 3C reception data to eliminate the 180° azimuth ambiguity of dipole reflection imaging logging (Gong et al. 2015). However, data measured with current tools cannot be used with their method because only the vector receiver is capable of obtaining the displacement. Therefore, the method can only be verified after the development of a new acoustic logging tool. Qiao et al. proposed an acoustic phased-arc array transmitter with azimuthal directivity (Qiao et al. 2006, 2008, 2009); Che et al. numerically simulated the acoustic field in fluid-filled open holes, cased holes and formations generated by phased-arc array transmitters (Che and Qiao 2009; Che et al. 2010, 2014); and Wu et al. investigated the radiation characteristics of a phase-combined arc array transmitter that can be used in 3D acoustic well logging (Wu et al. 2013). However, the above studies all focused on the transmitter itself and were relatively simple because they did not consider other sections, such as corresponding circuits and tool bodies.

In the current study, we designed 3D acoustic transmitter stations with circuits and bodies. These stations are composed of a phased-arc combined array that consists of dozens of independent transducers. The 3D acoustic transmitter stations can be used directly downhole with other tool sections for azimuthal acoustic reflection well logging. We also tested and analyzed the azimuthal performance of the transmitter stations in the laboratory.
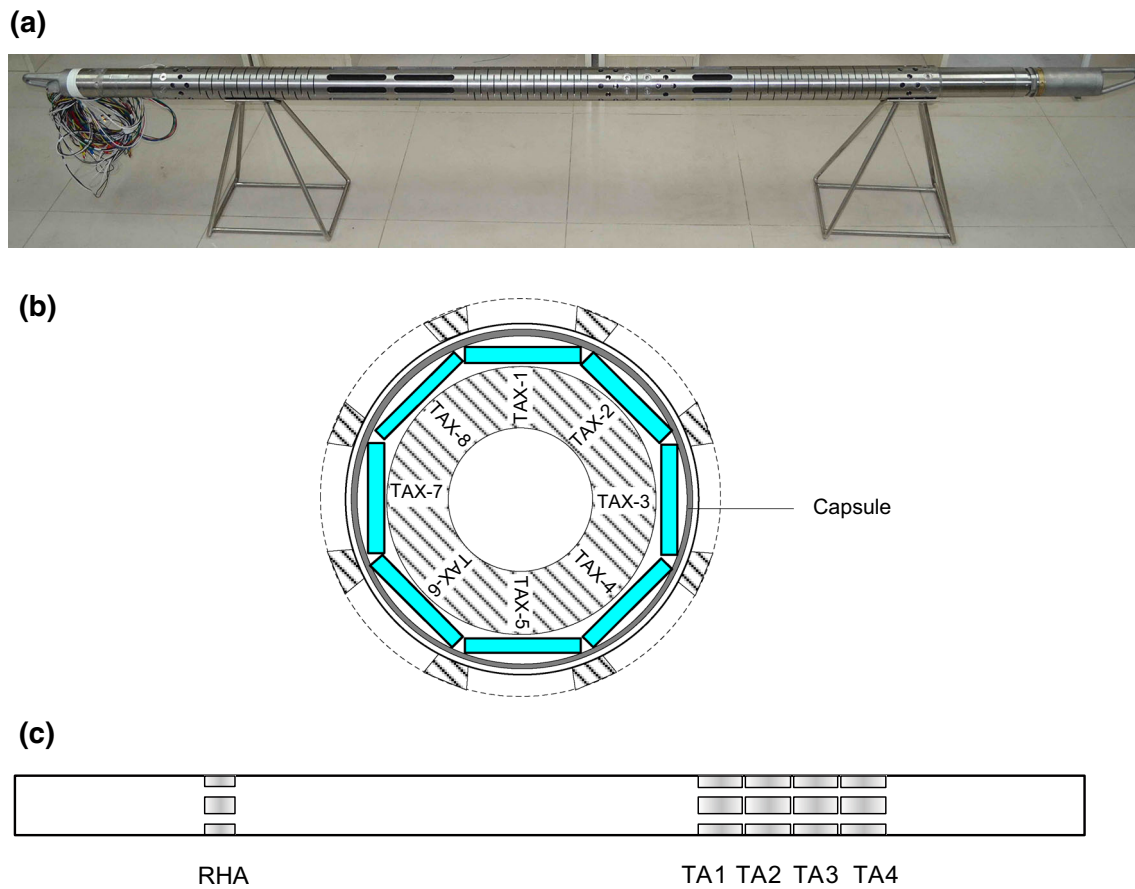
2 3D acoustic transmitter stations

Three-dimensional acoustic transmitter stations (Fig. 1) are the primary modules used by tools for azimuthal acoustic reflection well logging. The 3D structure consisting of four first-level subarrays that are evenly spaced along an axis is shown in Fig. 1a. A first-level subarray (Fig. 1b) is called a transmitter station, and it consists of eight elements that are distributed in a circle and numbered clockwise as TAx-1, TAx-2, TAx-3, TAx-4, TAx-5, TAx-6, TAx-7, and TAx-8, with x ranging from 1 to 4; thus, the four transmitter stations have a total of 32 independent transducers. The mandrel is made of steel and located inside the eight elements. The mandrel and the eight elements are sealed in a capsule and filled with silicone oil. The steel body near the elements is slotted to allow more acoustic energy to radiate into the borehole fluid. The four transmitter stations, which are numbered TA1, TA2, TA3, and TA4, are spaced 104 mm apart along the axis of the stations. Each of the four elements located along the axis in the same circumferential direction contains a phased linear array, which is defined as a second-level subarray. In each transmitter station, three adjacent elements constitute a third-level subarray. Therefore, one transmitter station can be recombined into eight three-element, third-level subarrays numbered clockwise as SUBx-1, SUBx-2, SUBx-3, SUBx-4, SUBx-5, SUBx-6, SUBx-7, and SUBx-8. The four third-level subarrays situated along the axis in the same circumferential direction consist of a combined arc array. The combined arc arrays are numbered clockwise as CAR-1, CAR-2, CAR-3, CAR-4, CAR-5, CAR-6, CAR-7, and CAR-8.

A 32-channel excitation circuit is integrated near the transmitter stations. Direct excitation with high-voltage pulses is applied to accurately control the pulse width, delay, polarity, and amplitude of each array element. When this circuit is controlled through a phased delay, the 3D acoustic transmitter stations can scan radiating acoustic energy with a circumferential stepping angle of 45° and an axial stepping angle of 1°. This pulse radiation mode can typically be used in azimuthal acoustic reflection logging tools. The main frequency is approximately 15 kHz. The excitation signal is a square wave with a signal width of one-half of the transducer main frequency reciprocal.

3 Experimental setup

The experimental setup for the 3D acoustic transmitter stations is depicted in Fig. 2. The transmitter stations are placed in a 5 m × 5 m × 4 m pool with a standard hydrophone. The hydrophone is moved and accurately

(a)

(b)

(c)

RHA   TA1 TA2 TA3 TA4

Fig. 1 **a** A photo of the 3D acoustic transmitter stations, **b** sketch of the element distribution of one transmitter station, and **c** 2D structure sketch of the 3D acoustic transmitter stations
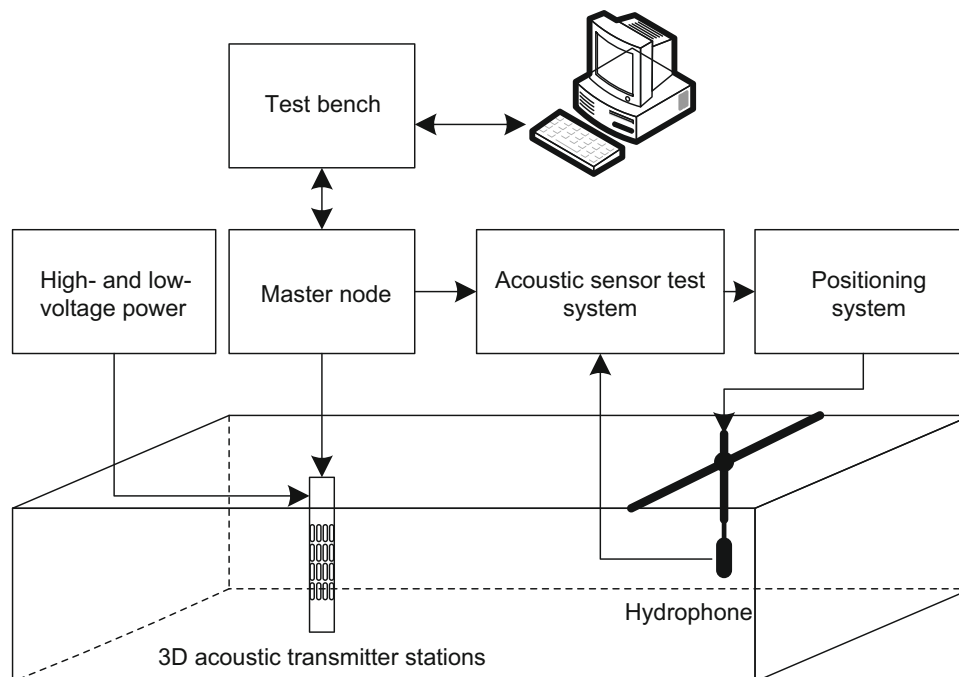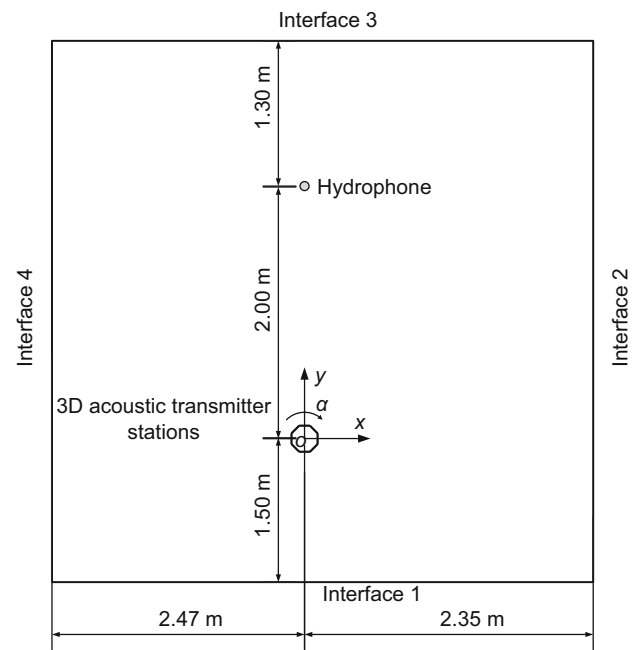

Fig. 2 Experimental setup for the 3D acoustic transmitter stations

positioned using a positioning system with four degrees of freedom. The test bench is an Ethernet-based embedded testing system that is specially designed to simulate logging ground controls and measurements. This system communicates with the 3D acoustic transmitter stations through a controller area network (CAN) bus. The master node is the main control circuit of the tool for azimuthal acoustic reflection logging. The programs are operated in the same mode used for actual well logging except that the codes utilized to control the acquisition nodes are blocked. For synchronicity with the acoustic sensor test system, an indicator signal SYN is introduced with the same synchronizing frame as the tool control bus. The test bench ensures the functionality of the 3D excitation circuits under the control of the host computer. The acoustic sensor test system initiates a synchronized collection in response to the synchronization signal. The hydrophone acquires data several times at each position and then moves along a predetermined trajectory under the control of the positioning system.

During experimental measurements, the 3D acoustic transmitter stations radiate acoustic waves that are then received by the hydrophone. The transmitter is maintained at a fixed height, whereas the hydrophone position is adjusted via the positioning system to situate the hydrophone at the same horizontal plane as the geometric center of the transmitter. The shortest distance to the water surface is 0.75 m, and the interval is 2.00 m. The transmitter stations are manually rotated clockwise to ensure that the normal exterior of each radiating surface of the eight elements is aligned with the geometric center of the hydrophone. The stepping angle α is 45°. The horizontal layout of the transmitter and the receiver during the experimental measurements is shown in Fig. 3. A coordinate system (*xoy*) is constructed with the axis center of the 3D acoustic transmitter stations as the origin. The positive direction of the *y* axis points to the geometric center of the hydrophone. Initially, the northern direction of the transmitter stations is parallel to the positive direction of the *y* axis. The excitation signal is a 600 V square wave with a pulse width of 30 μs. The time delay of the third-level subarray is 6 μs when the previous calculation method is applied (Che et al. 2010).

To measure the horizontal directivity of each combined arc array, which is shown in Fig. 4a, we first fix the position of the 3D acoustic transmitter stations (T) and excite these stations to radiate acoustic energy. The hydrophone moves along an arc with a radius of 2.00 m and central angle of 120° in the *xy* plane. The center of this plane is the geometric center (*o*) of the transmitter stations. The hydrophone receives acoustic waves generated by T at 61 evenly distributed positions along the arc, and the opening angle between each pair of adjacent receiver positions is 2° with respect to *o*. The hydrophone moves along an arc with

Fig. 3 Horizontal layout of the transmitter and receiver during experimental measurements for the 3D acoustic transmitter stations

a radius of 2.00 m and a central angle of 67° to measure vertical directivity. The geometric center (*o*) of the transmitter stations is the origin of the *xoz* plane as depicted in Fig. 4b. The hydrophone receives the acoustic waves generated by T at 68 evenly distributed positions along the arc, and the opening angle of each pair of adjacent receiver positions is 1° with respect to *o*.

4 Experimental results

First, we tested each of the elements in the four transmitter stations (i.e., TA1, TA2, TA3, and TA4). We then examined each of the third-level subarrays of the four transmitter stations and analyzed all of the measured waveforms as well as their corresponding spectra. Furthermore, we measured the horizontal directivity of the third-level subarrays as well as the horizontal and vertical directivities of the combined arc arrays.

4.1 Individual elements

When testing the individual elements, the height and angle of the 3D acoustic transmitter stations were adjusted to ensure that the tested element is on the same horizontal level as the hydrophone (the hydrophone is in the normal direction of the element radiating surface). Each of the elements, from TA1 to TA4, was excited to generate acoustic energy. The hydrophone was situated 2.00 m away from the tested element. We calculated the average
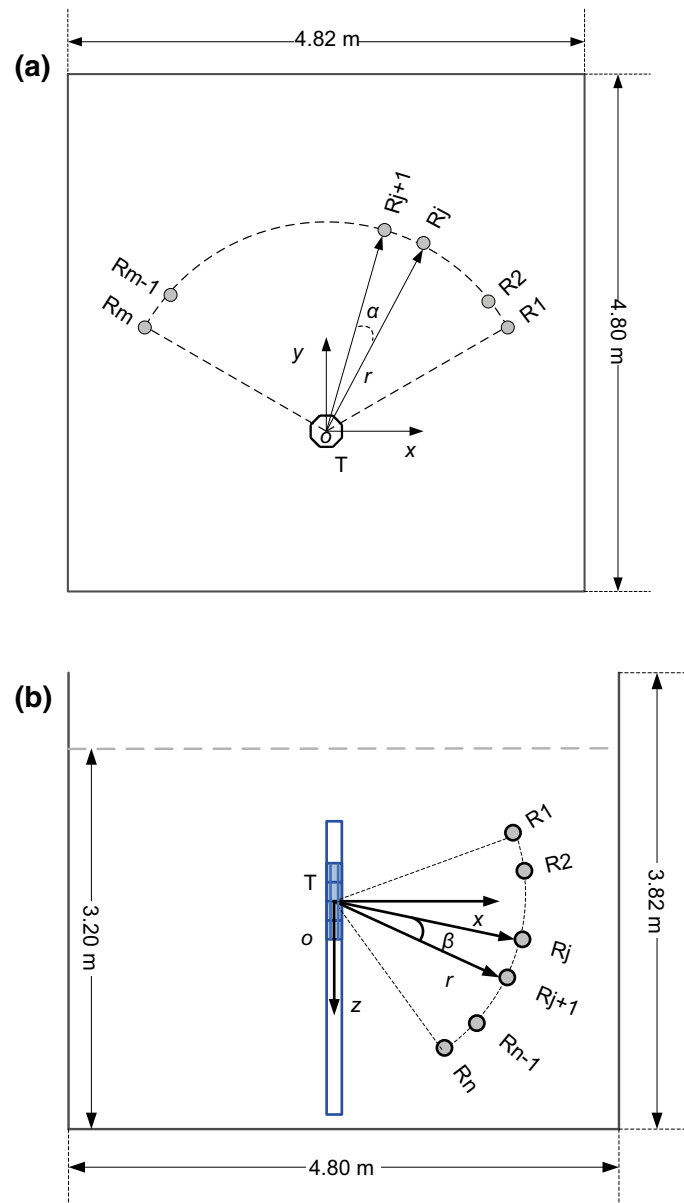
Fig. 4 Distribution of the transmitter and receiver for the **a** horizontal and **b** vertical directivity measurements

basic frequencies, average peak–peak voltages, and average peak–peak sound pressures of the direct waves for each transmitter station as shown in Table 1. Figures 5 and 6 display the direct waves received by the hydrophone and their corresponding spectra when transmitter stations TA1

and TA2 are excited, respectively. The acoustic waves generated by the elements of the transmitter stations exhibit almost identical waveform patterns with slightly different amplitudes. The transmission performance of the elements is consistent.

Table 1 Average basic frequencies, average peak–peak voltages, and average peak–peak sound pressures of the direct waves at 2.00 m intervals when testing each element of the four transmitter stations

Average value	TA1	TA2	TA3	TA4
Basic frequency, kHz	14.58	14.44	14.60	14.42
Peak–peak voltage, mV	21.45	22.24	23.75	21.30
Peak–peak sound pressure, Pa	1178	1222	1305	1170
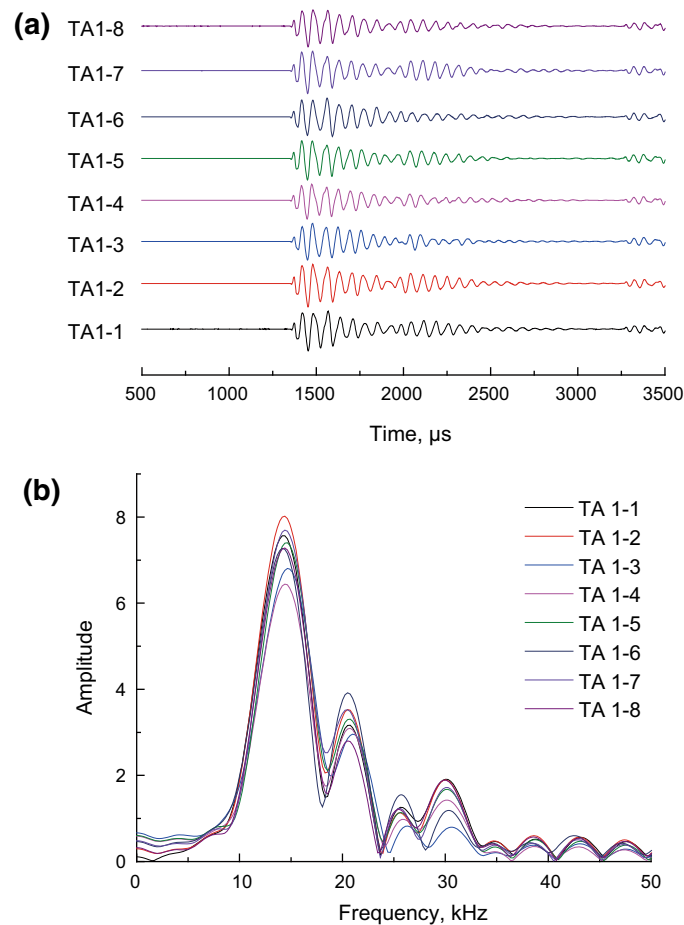
Fig. 5 **a** Experimental waveforms in the time-domain received by the hydrophone and **b** corresponding spectra when each of the TA1 elements radiates acoustic energy

4.2 Third-level subarrays

A transducer composed of the three adjacent elements of a transmitter station is considered to be a third-level subarray. To test the third-level subarrays, we adjusted the height and angle of the 3D acoustic transmitter stations to position the third-level subarray on the same horizontal plane as the hydrophone. In addition, the hydrophone was adjusted to the normal direction of the center element radiating surface of the third-level subarray. We separately excited all eight third-level subarrays of TA1, TA2, TA3, and TA4. The average basic frequencies, average peak–peak voltages, and average peak–peak sound pressures calculated from the waveforms in 2.00 m intervals are shown in Table 2. Figures 7 and 8 show the direct waves received by the hydrophone and their corresponding spectra when the third-level subarrays of TA1 and TA2 are excited, respectively. The waveforms generated by the third-level subarrays of the arc array exhibit almost identical patterns. Moreover, the spectra of the third-level

subarrays are identical with slightly different amplitudes. The radiation performance of the third-level subarrays is nearly consistent.

We also separately tested the horizontal directivities of the four third-level subarrays in the same circumferential direction. Elements 4, 5, and 6 were set as the centers of the third-level subarrays. Figure 9a–d shows the time-domain waveforms received by the hydrophone at different azimuth φ values when the four subarrays are in the same circumferential direction, and element 5 is the center. The direct wave amplitude is distributed symmetrically around the axis of the main lobe; this amplitude peaks at 0° and decreases gradually from 0° on both sides.

The amplitude of the time-domain waveforms was also analyzed to obtain the directivity curves (Fig. 10). This amplitude is shown in Fig. 9 during a time window of approximately 1320–1900 μs. The direction of the main radiated beam points consistently to 0° for all four third-level subarrays in the same circumferential direction when element 5 is the center. The radiated acoustic beams are
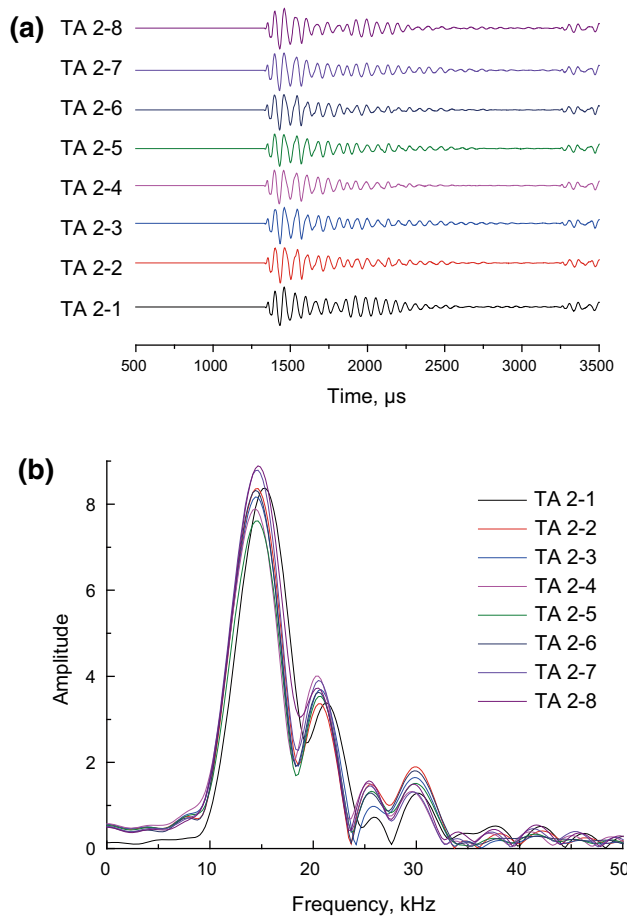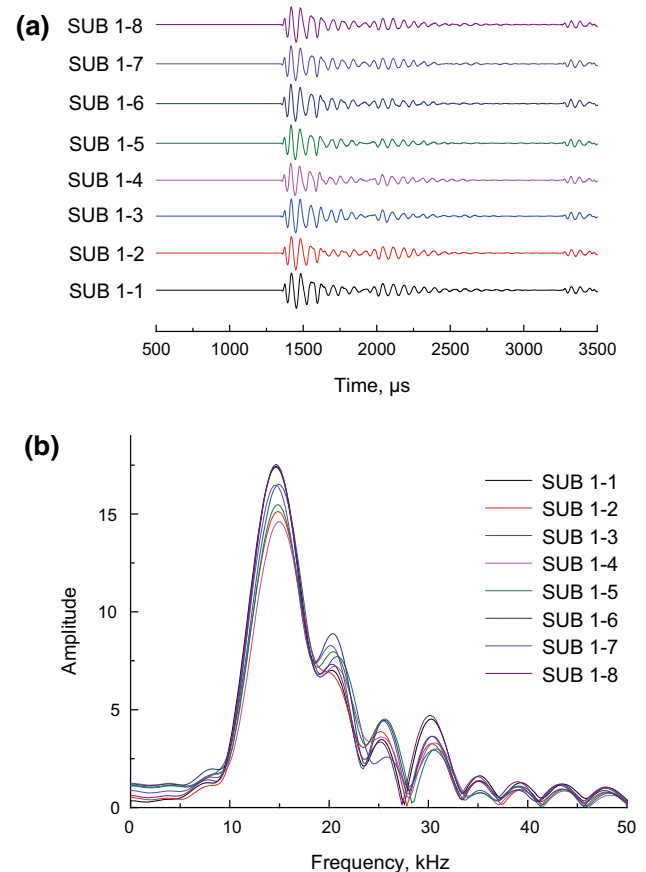
Fig. 6 **a** Experimental waveforms in the time-domain received by the hydrophone and **b** corresponding spectra when each of the TA2 elements radiates acoustic energy

Fig. 7 **a** Experimental waveforms in the time-domain received by the hydrophone and **b** corresponding spectra when each of the TA1 subarrays radiates acoustic energy

distributed almost symmetrically around the main lobes. In addition, sound pressures and 3-dB beam widths are similar in the main lobe direction. Table 3 displays the peak–peak voltages, main frequencies, peak–peak sound pressures, and 3-dB beam widths of the direct waves generated by each of the third-level subarrays excited in the main lobe direction.

4.3 Combined arc arrays

When acoustic energy is radiated to the formations around a borehole during azimuthal acoustic reflection logging, the vertical deflection angle of the main acoustic beam radiated

by the transmitter is generally smaller than the first critical angle of the incident acoustic wave on the borehole wall from the borehole fluid. Thus, additional acoustic wave energy can enter the formation; this occurrence deepens the investigation and improves the signal-to-noise ratios of the useful signals. The main lobe of an acoustic beam radiated by a phased-combined arc array has a certain angular width. Therefore, the deflection angle of the main beam in the vertical plane is designed at approximately half of the first critical angle when a combined arc array is employed to radiate a 3D acoustic field to the formation. When measuring the directivity of the combined arc array, the method of Wu et al. was adopted to calculate the delay between different elements (Wu et al. 2013). The vertical

Table 2 Average basic frequencies, average peak–peak voltages, and average peak–peak sound pressures of the direct waves at 2.00 m intervals

Average value	TA1	TA2	TA3	TA4
Basic frequency, kHz	15.06	14.82	15.00	14.76
Peak–peak voltage, mV	52.18	56.27	59.94	52.47
Peak–peak sound pressure, Pa	2867	3092	3293	2883
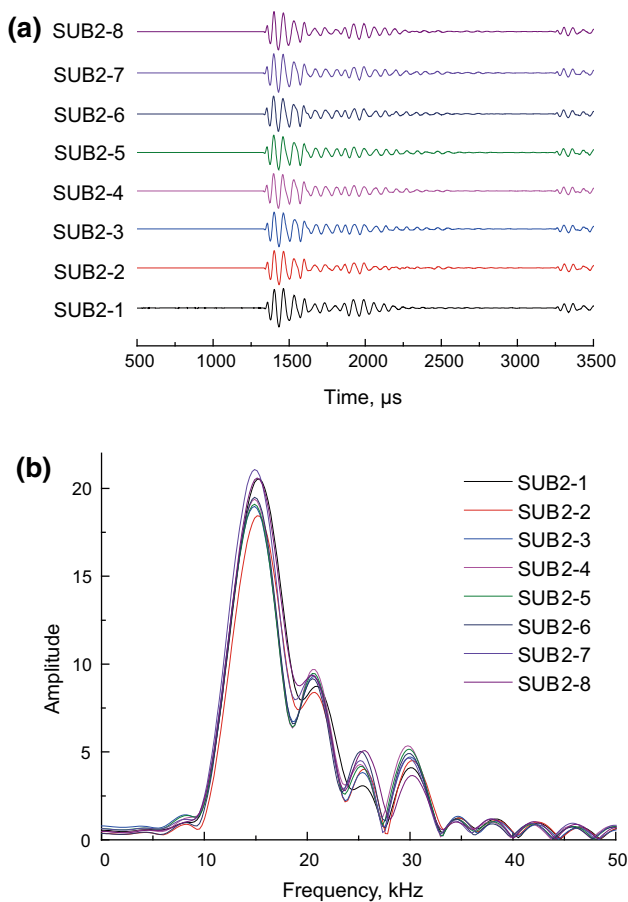
Fig. 8 a Experimental waveforms in the time-domain received by the hydrophone and **b** corresponding spectra when each of the TA2 subarrays radiates acoustic energy

deflection angle of the main acoustic beam is assumed to be $\theta_0 = 16°$. The horizontal directivity of each combined arc array in the *xoy* plane was first measured, and then the vertical directivity in the vertical plane $\varphi = 0°$ was measured; this plane is situated at the horizontal maximum direction of the main lobe. Figure 11 displays the time-domain waveforms received by the hydrophone at different azimuths when the combined arc array CAR-6 is excited. The distribution of the direct wave amplitude is symmetric in the *xoy* plane, with a peak at 0°. These results are consistent with the distribution of the direct wave amplitudes of the third-level subarrays. In the $\varphi = 0°$ plane, the direct wave amplitude changes with deflection angle variations. The amplitude peaks at a deflection angle of 14°; thus, the main lobe of radiation is steered at 14°.

Figures 12 and 13 show the experimental horizontal and vertical directivity curves of the combined arc arrays. The main lobe of the radiated acoustic beams for the three combined arc arrays points to approximately $\varphi = 0°$. The beams are distributed symmetrically around the direction of the main lobes, with a 3-dB beam width that ranges from

59° to 67°. The main lobe in the vertical plane deflects along the direction of $\theta = 14°$, which almost corresponds to the designed deflection angle of 16°. The 3-dB beam width is only 11°. Thus, the 3D acoustic transmitter stations exhibit acceptable azimuthal directivity. Because the phased-combined arc array transmitter radiates acoustic energy in a certain azimuth with a specific angle width, acoustic energy can then be radiated to a 3D space through scanning by the excitation of different combined arc arrays.

The time-domain waveforms received by the hydrophone at 2.00 m intervals were analyzed when each combined arc array radiates acoustic energy in the deflected direction. A statistical analysis was also performed on the time-domain waveforms and their corresponding spectra. Table 4 shows the peak–peak voltages, main frequencies, and peak–peak sound pressures when the three combined arc arrays are excited separately. Overall, the three combined arc arrays exhibit good transmission performance.

4.4 Discussion

As shown in Figs. 8b, 6b, and the corresponding tables, the third-level subarrays (three-element arc arrays) radiate acoustic waves with amplitudes that are approximately 2.5 times greater than those of the acoustic waves radiated by an individual element. The observed spectra are essentially identical. In addition, the 3-dB beam width of the vertical directivity that is radiated by the third-level subarray is approximately 60°, which reveals that three-element arc arrays can radiate focused acoustic energy in a certain azimuthal range while radiating weak acoustic energy in other directions.

The combined arc array radiates acoustic waves with similar spectra and amplitudes that are approximately 3.4 times greater than those of the acoustic waves radiated by a third-level subarray as shown in Figs. 11b and 8b as well as the corresponding tables. Figure 12 indicates that the horizontal directivity of the 3D acoustic transmitter stations displays a 3-dB beam width of less than 60°, which indicates that the system exhibits a high capacity for directional radiation. The results revealed that acoustic energy radiated in a certain azimuthal range was effectively increased by increasing the number of three-element arc arrays along the axial direction, and these results will help increase the amount of radiated acoustic energy that enters the formation when the transducer is used downhole.

Figure 13 shows that the 3-dB beam width in the vertical plane is only 11° when the radiated acoustic beam is deflected by 14° in the vertical plane. Such conditions maximize the amount of radiated acoustic wave energy that enters a formation surrounding a fluid-filled borehole. The results reveal that increasing the number of arc arrays along
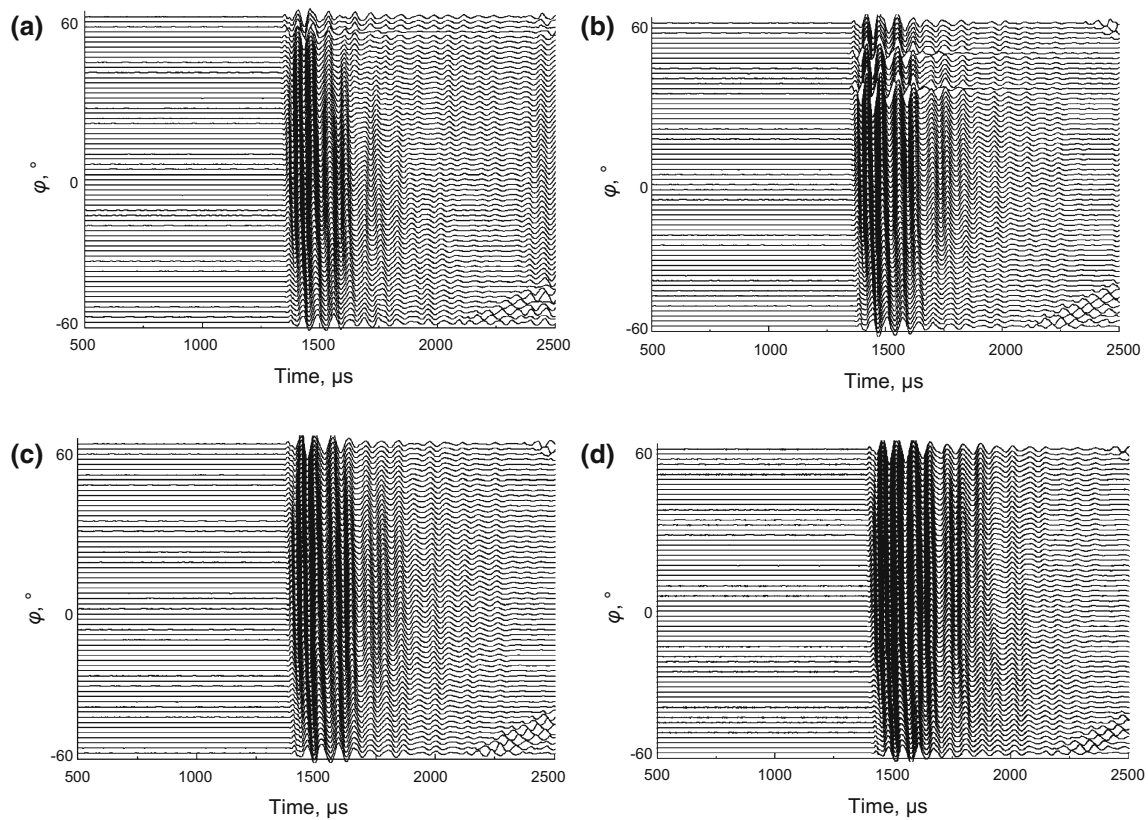
Fig. 9 Time-domain waveforms received by the hydrophone at different azimuth φ values when the four subarrays radiate in the same circumferential direction and element 5 is the center. **a** SUB1-5, **b** SUB2-5, **c** SUB3-5, and **d** SUB4-5
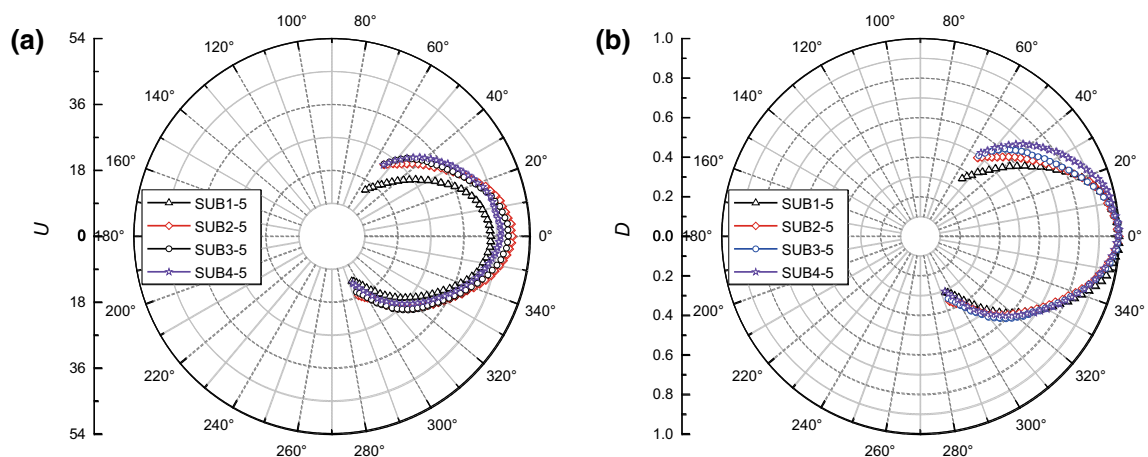
Fig. 10 Horizontal directivities of the third-level subarrays with element 5 as the center. **a** without normalization and **b** with normalization. D is a dimensionless variable

the axial direction can increase the acoustic energy radiated in a certain azimuthal range and also improve the vertical radiation directivity of the transducer. Thus, it is possible to impinge the radiated acoustic wave onto the borehole wall at an incident angle that is smaller than the first critical angle when using the downhole 3D acoustic transmitter stations. Therefore, the acoustic energy radiated by the

transducer almost wholly converts to formation compressional energy.

The 3D acoustic transmitter stations can radiate acoustic waves in any desired direction by controlling the phase and amplitude of the 32-channel excitation pulse. Therefore, azimuthal acoustic reflection logging can be realized with the proposed transmitter stations.

Table 3 Peak–peak voltages, main frequencies, peak–peak sound pressures, and 3-dB beam width of the direct waves generated by each of the third-level subarrays

Numbering	Peak–peak voltage, mV	Main frequency, kHz	Peak–peak sound pressure, Pa	3-dB beam width
SUB1-4	31.32	14.89	1721	45°
SUB2-4	47.84	14.65	2629	65°
SUB3-4	48.04	14.40	2639	59°
SUB4-4	42.69	14.65	2346	71°
SUB1-5	43.40	14.65	2384	61°
SUB2-5	49.28	14.40	2708	63°
SUB3-5	48.26	14.65	2651	67°
SUB4-5	46.18	14.40	2537	73°
SUB1-6	42.50	14.89	2335	76°
SUB2-6	48.83	14.65	2683	65°
SUB3-6	50.47	14.65	2773	58°
SUB4-6	48.34	14.40	2656	57°
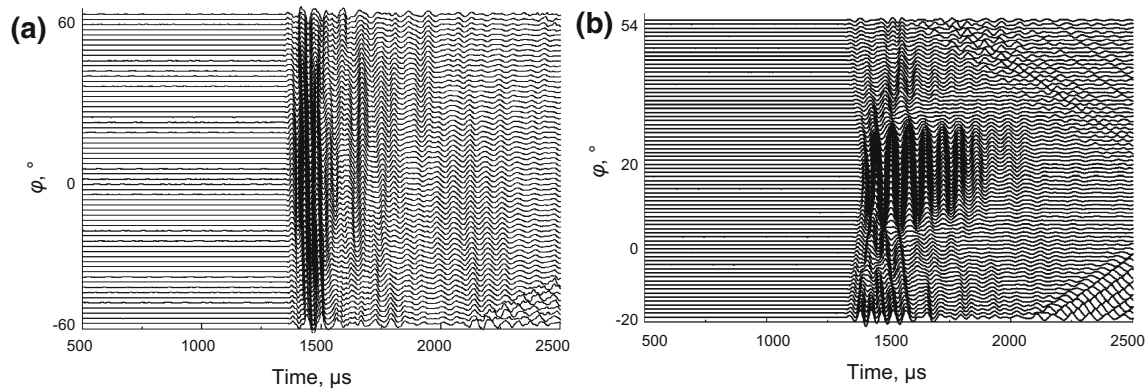
Fig. 11 Waveforms in the time-domain received by the hydrophone in different azimuths when the combined arc array CAR6 radiates acoustic energy; **a** *xoy* plane and **b** $\varphi = 0°$ plane
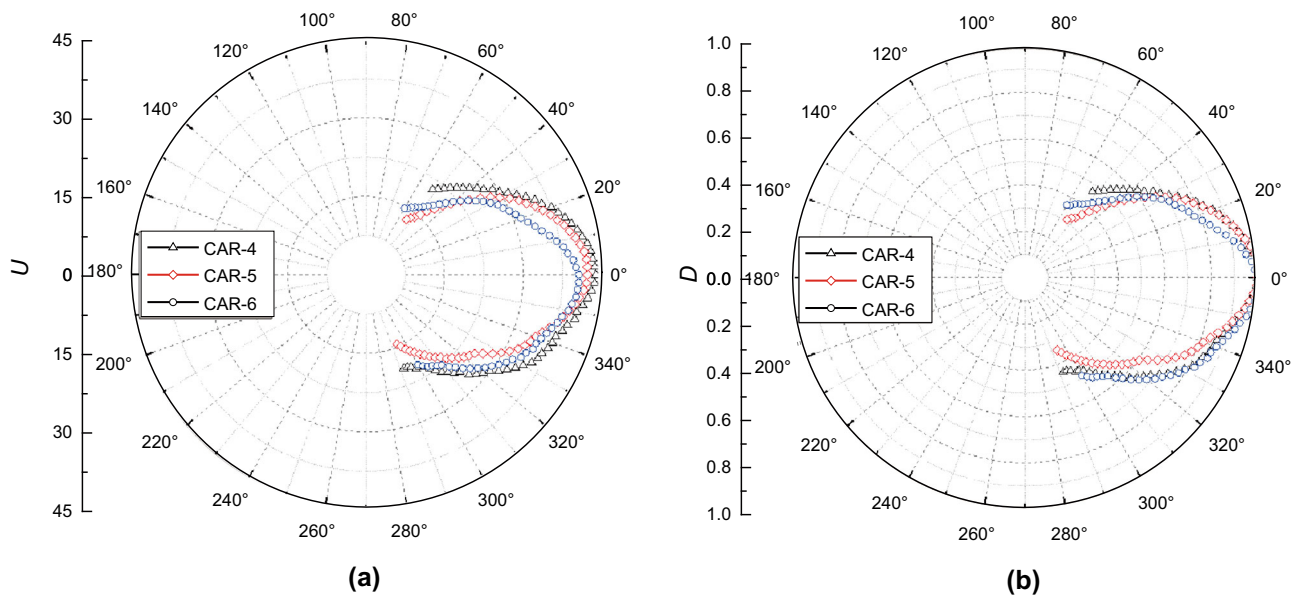
Fig. 12 Radiation directivity curves of the combined arc arrays in the 3D acoustic transmitter stations; **a** without normalization and **b** with normalization
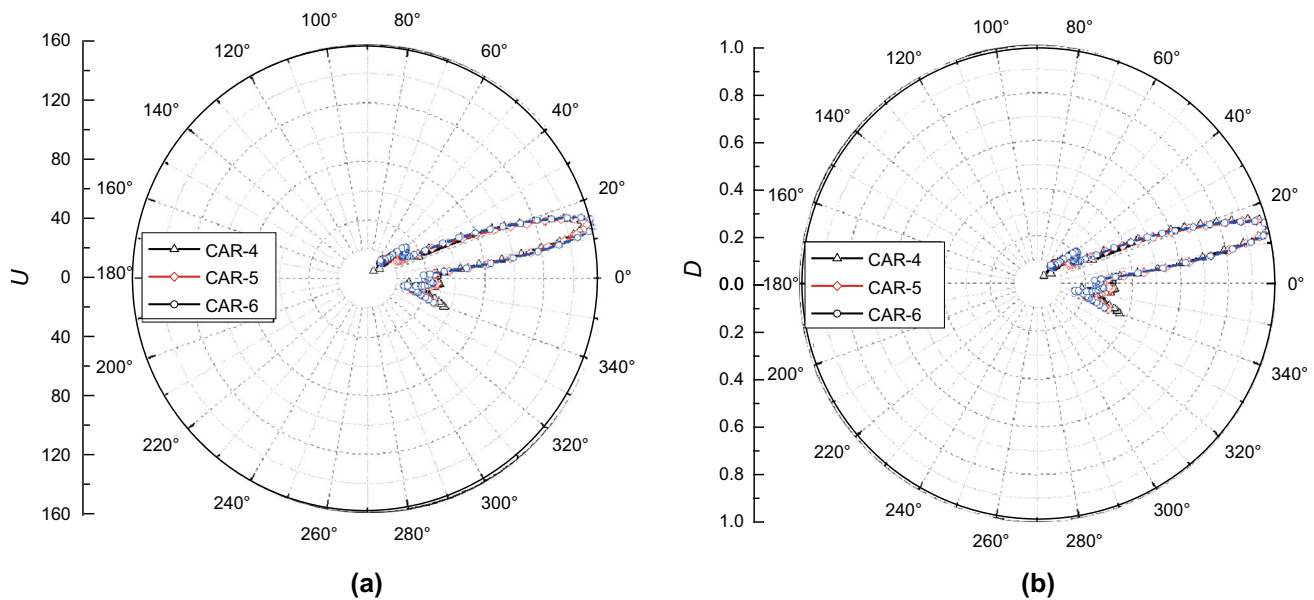
Fig. 13 Vertical directivities of the combined arc arrays in the 3D acoustic transmitter stations; **a** without normalization and **b** with normalization

Table 4 Peak–peak voltages, main frequencies, and peak–peak sound pressures of the combined arc arrays

Numbering	Peak–peak voltage, mV	Main frequency, kHz	Peak–peak sound pressure, Pa
CAR-4	151.29	14.40	8314
CAR-5	153.31	14.40	8424
CAR-6	159.59	14.40	8770

5 Conclusions

Here, we propose 3D acoustic transmitter stations with corresponding circuits and bodies for azimuthal acoustic reflection well logging. The transmitter stations consist of three-level subarrays that are evenly spaced along an axis, and each element is an individual transducer. We measured the azimuthal performance of the transmitter stations, including the vertical and horizontal directivity curves of the combined arc arrays.

The measured waveforms and their corresponding spectra show that the waveform pattern and the radiation performance levels of the individual elements and the third-level subarrays are almost consistent except for slight differences in amplitude. When the four third-level subarrays in the same circumferential direction are excited by a "quasi-square wave" pulse signal with a pulse width of 30 μs and a voltage of 600 V, the main lobes of the radiation acoustic beams point to 0° in the horizontal plane. The acoustic beams, which exhibit a 3-dB beam width that ranges from 59° to 67°, are distributed symmetrically around the main lobes. Furthermore, the horizontal directivities of the four third-level subarrays in the same circumferential direction are nearly consistent. The main lobe

of the acoustic beams for the combined arc arrays is steered by 14° in the vertical plane with a 3-dB beam width of 11° during individual operation. The combined arc arrays of the proposed 3D acoustic transmitter stations are also consistent, which indicates that the system can be used in azimuthal acoustic reflection logging.

Three-element arc arrays can radiate focused acoustic energy in a certain azimuthal range while radiating only weak acoustic energy in other directions. Increasing the number of arc arrays along the axial direction can increase the acoustic energy radiated in a certain azimuthal range and also improve the vertical radiation directivity of the transducer. The radiated acoustic wave can be made to impinge onto the borehole wall at an incident angle that is smaller than the first critical angle when using the 3D acoustic transmitter stations downhole. Therefore, the acoustic energy radiated by the transducer almost wholly converts to the formation compressional energy.

The exploration accuracy of the proposed 3D acoustic transmitter stations must be calibrated further for application in downhole tools for oil field tests. However, the large number of required transducers complicates the electronic circuits of the transmitter stations. Thus, accurate phase control is necessary to ensure good azimuthal performance.

References

Al Rougha HAB, Sultan A, Haldorsen J, et al. Integration of microelectrical and sonic reflection imaging around the borehole offshore UAE. Paper IPTC 11021 presented at International Petroleum Technology Conference, Doha, Qatar; 21–23 Nov 2005.

Chai XY, Zhang WR, Wang GQ, et al. Application of remote exploration acoustic reflection imaging logging technique in fractured reservoirs. Well Logging Technol. 2009;33(6):539–43 (in Chinese).

Chang C, Hoyle D, Watanabe S, et al. Localized maps of the subsurface. Oilfield Rev. 1998;10:56–66.

Che XH, Qiao WX. Numerical simulation of an acoustic field generated by a phased arc array in a fluid-filled borehole. Pet Sci. 2009;6(3):225–9.

Che XH, Qiao WX, Ju XD. Characteristics of the acoustic field generated by an acoustic phased arc array transmitter in the borehole formation. Acta Pet Sin. 2010;31(2):343–6 (in Chinese).

Che XH, Qiao WX, Wang RJ, et al. Numerical simulation of an acoustic field generated by a phased arc array in a fluid-filled cased borehole. Pet Sci. 2014;11(3):385–90.

Ellis D, Engelman B, Fruchter J, et al. Environmental applications of oilfield technology. Oilfield Rev. 1996;8:44–57.

Esmersoy C, Chang C, Kane MR, et al. Sonic imaging: a tool for high-resolution reservoir description. 67th SEG Annual Meeting, Expanded Abstracts. 1997. pp. 278–281.

Esmersoy C, Chang C, Kane M, et al. Acoustic imaging of reservoir structure from a horizontal well. Lead Edge. 1998;17(7):940–6.

Gong H, Chen H, He X, et al. Eliminating the azimuth ambiguity in single-well imaging using 3C sonic data. Geophysics. 2015;80(1):A13–7.

Haldorsen JBU, Johnson DL, Plona T, et al. Borehole acoustic waves. Oilfield Rev. 2006;18:34–43.

Haldorsen J, Voskamp A, Thorsen R, et al. Borehole acoustic reflection survey for high resolution imaging. 76th SEG Annual Meeting, Expanded Abstracts. 2006b. pp. 314–18.

Haldorsen JBU, Zhu FP, Hirabyashi N, et al. Borehole acoustic reflection survey (BARS) using full waveform sonic data. First Break. 2010;28:33–8.

Hornby BE. Imaging of near-borehole structure using full-waveform sonic data. Geophysics. 1989;54(6):747–57.

Jervis M, Bakulin A, Tonellot TL, et al. High-resolution seismic imaging from a single borehole to detect a nearby well. Paper SEG 2012-0963.1 presented at 72th SEG Annual Meeting, Expanded Abstracts, Las Vegas; 4–9 Nov 2012.

Li LS, Wang LJ, Wang ZY, et al. Application of the data from distant detection acoustic imaging well logging. World Well Logging Technol. 2008;23(4):14–5 (in Chinese).

Maia W, Rubio R, Junior F, et al. First borehole acoustic reflection survey mapping a deepwater turbidite sand. 76th SEG Annual Meeting, Expanded Abstracts. 2006. pp. 1757–61.

Patterson D, Tang XM, Ratigan J. High-resolution borehole acoustic imaging through a salt dome. 78th SEG Annual Meeting, Expanded Abstracts. 2008. pp. 319–23.

Pistre V, Kinoshita K, Endo T, et al. A modular wireline sonic tool for measurements of 3D (azimuthal, radial, and axial) formation acoustic properties. SPWLA 46th Annual Logging Symposium, New Orleans, Louisiana; 26–29 Jun 2005.

Qiao WX, Ju XD, Chen XL, et al. Downhole acoustic arc array transmitter with controlled azimuthal directivity. China Patent ZL. 2006; 03137596. 0 (in Chinese).

Qiao WX, Che XH, Ju XD, et al. Acoustic logging phased arc array and its radiation directivity. Chin J Geophys. 2008;51(3):939–46 (in Chinese).

Qiao WX, Ju XD, Che XH. A kind of acoustic logging with phased arc array transducer. Well Logging Technol. 2009;33(1):22–5 (in Chinese).

Tang XM. Imaging near-borehole structure using directional acoustic-wave measurement. Geophysics. 2004;69(6):1378–86.

Tang XM, Zheng Y, Patterson D. Processing array acoustic logging data to image near-borehole geologic structures. Geophysics. 2007;72(2):87–97.

Tang XM, Wei ZT. Significant progress of acoustic logging technology: remote acoustic reflection imaging of a dipole acoustic system. Appl Acoust. 2012a;31(1):10–7 (in Chinese).

Tang XM, Wei ZT. Single-well acoustic reflection imaging using far-field radiation characteristics of a borehole dipole source. Chin J Geophys. 2012b;55(8):2798–807 (in Chinese).

Tang XM, Patterson D. Single-well S-wave imaging using multi-component dipole acoustic log data. Geophysics. 2009;74(6):211–23.

Wei ZT, Tang XM, Zhuang CX. P-wave remote acoustic imaging of a borehole dipole source radiation in an acoustically slow formation. Acta Pet Sin. 2013;33(5):905–13 (in Chinese).

Wu JP, Qiao WX, Che XH, et al. Experimental study on the radiation characteristics of downhole acoustic phased combined arc array transmitter. Geophysics. 2013;78(1):D1–9.

Yamamoto H, Haldorsen JBU, Mikada H, et al. Fracture imaging from sonic reflections and mode conversion. 69th SEG Annual Meeting, Expanded Abstracts, Houston, Texas; 31 Oct–5 Nov 1999.

Yamamoto H, Watanabe S, Mikada H, et al. Fracture imaging using borehole acoustic reflection survey. Proceedings of the 4th SEGJ International Symposium. 1998. pp. 375–82.

Yamamoto H, Watanabe S, Koelman JMV, et al. Borehole Acoustic reflection survey experiments in horizontal wells for accurate well positioning. Paper SPE/PS-CIM 65538 presented at SPE/PS-CIM International Conference on Horizontal Well Technology, Calgary, Alberta, Canada; 6–8 Nov 2000.

Zhang YD, Hu HS. A technique to eliminate the azimuth ambiguity in single-well imaging. Geophysics. 2014;79(6):D409–16.

Zhao XD, Li GY, Liu BZ. On transmitting transducer of far detecting acoustic logging tool. Well Logging Technology. 2004;28(6):540–2 (in Chinese).